The sun in neutrinos from Super-K

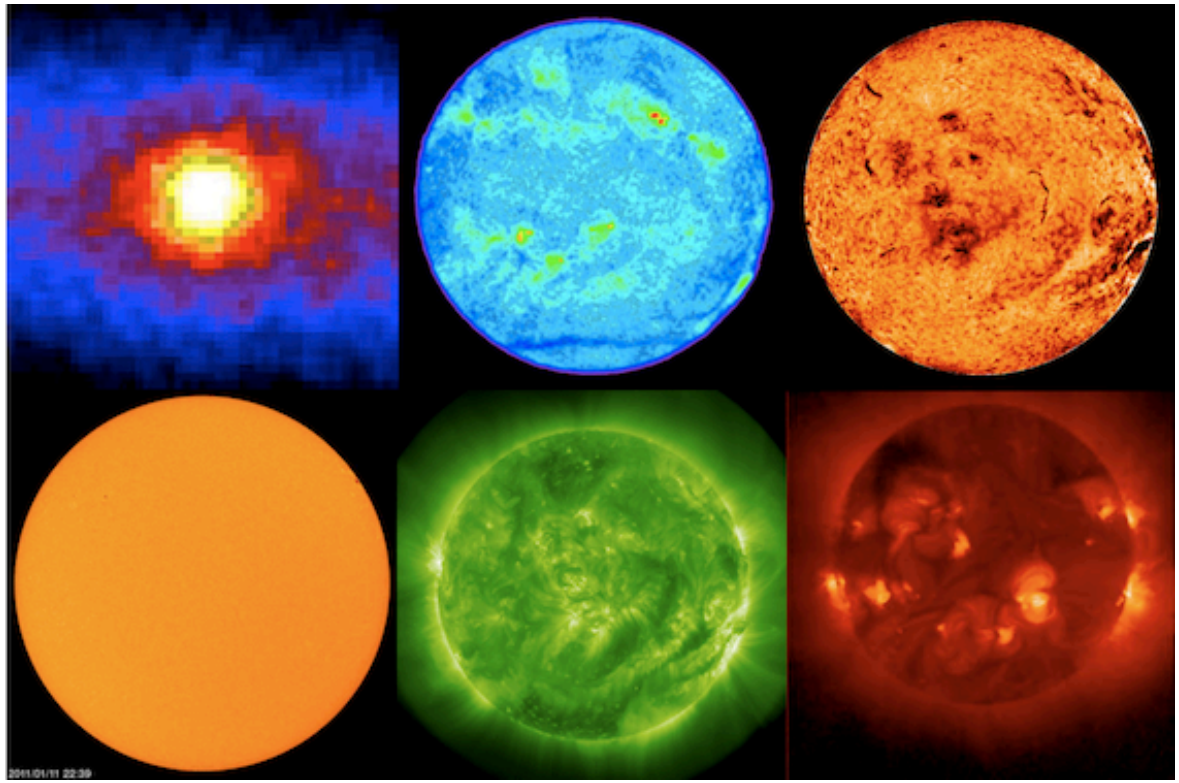

Figure 1: Images of the Sun: whereas the neutrino emission originates in the dense core of the Sun, photonic observations originate in the solar surface and atmosphere. From top left: Neutrino ‘image’ of the Solar core (Image credit: R. Svoboda, K. Gordan, LSU), radio emission from the solar atmosphere (Image credit: S. White, University of Maryland, NRAO/AUI), infrared image from the solar chromosphere (Image credit: National Solar Observatory, Kitt Peak/NOAO), visible image of the solar surface (Image credit: SOHO/ESA/NASA), extreme ultraviolet emission from the corona (Image credit: NASA/SDO/AIA), X-ray emission from the solar corona (Image credit: Yohkoh).

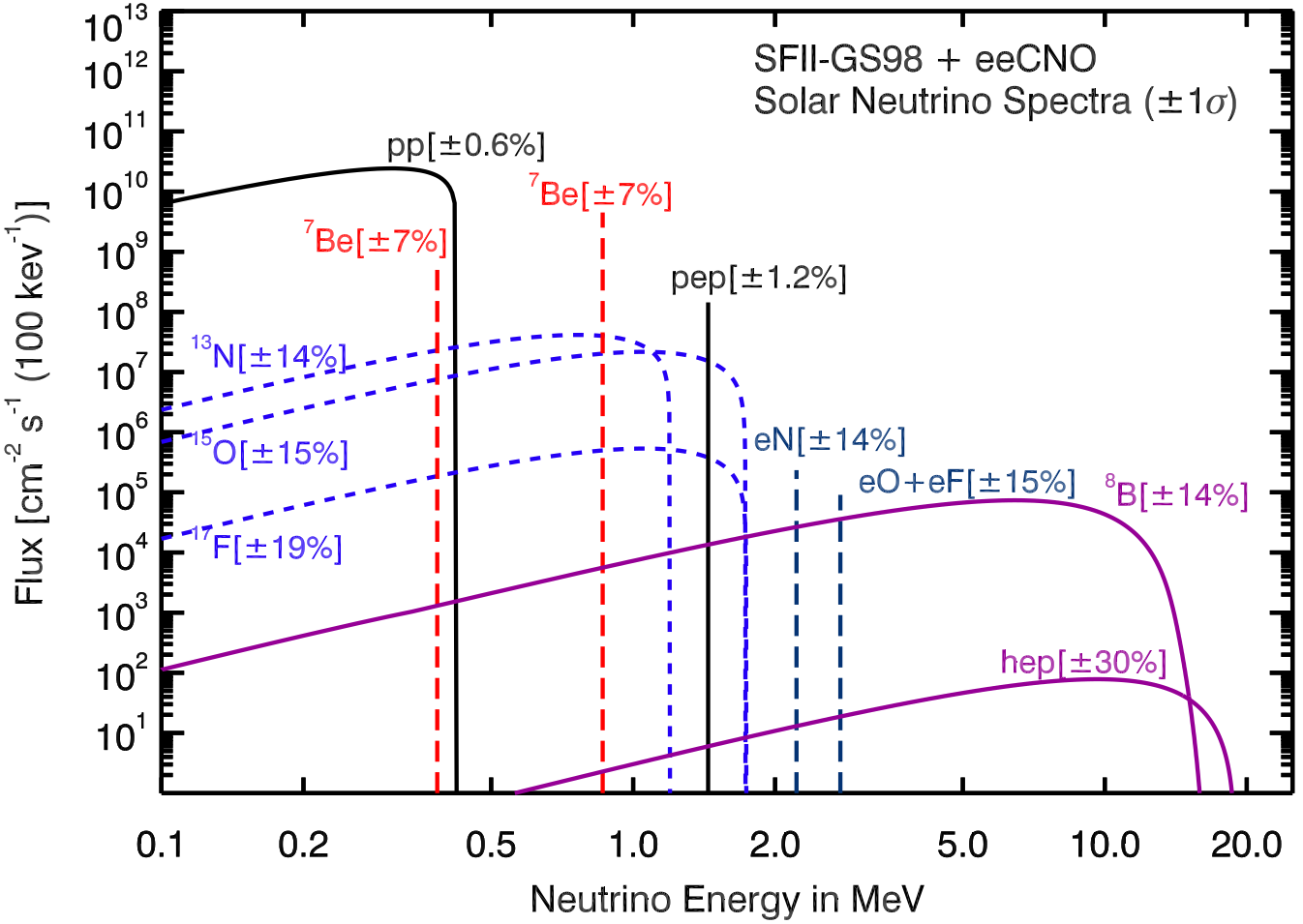

Figure 14.1: Spectrum of solar neutrino fluxes predicted by SSM calculation in [41]. In addition to standard fluxes, ecCNO neutrinos have been added based on [42]. Electron capture fluxes are given in $\mathrm{cm}^{-2}\mathrm{s}^{-1}$. Taken from [43]

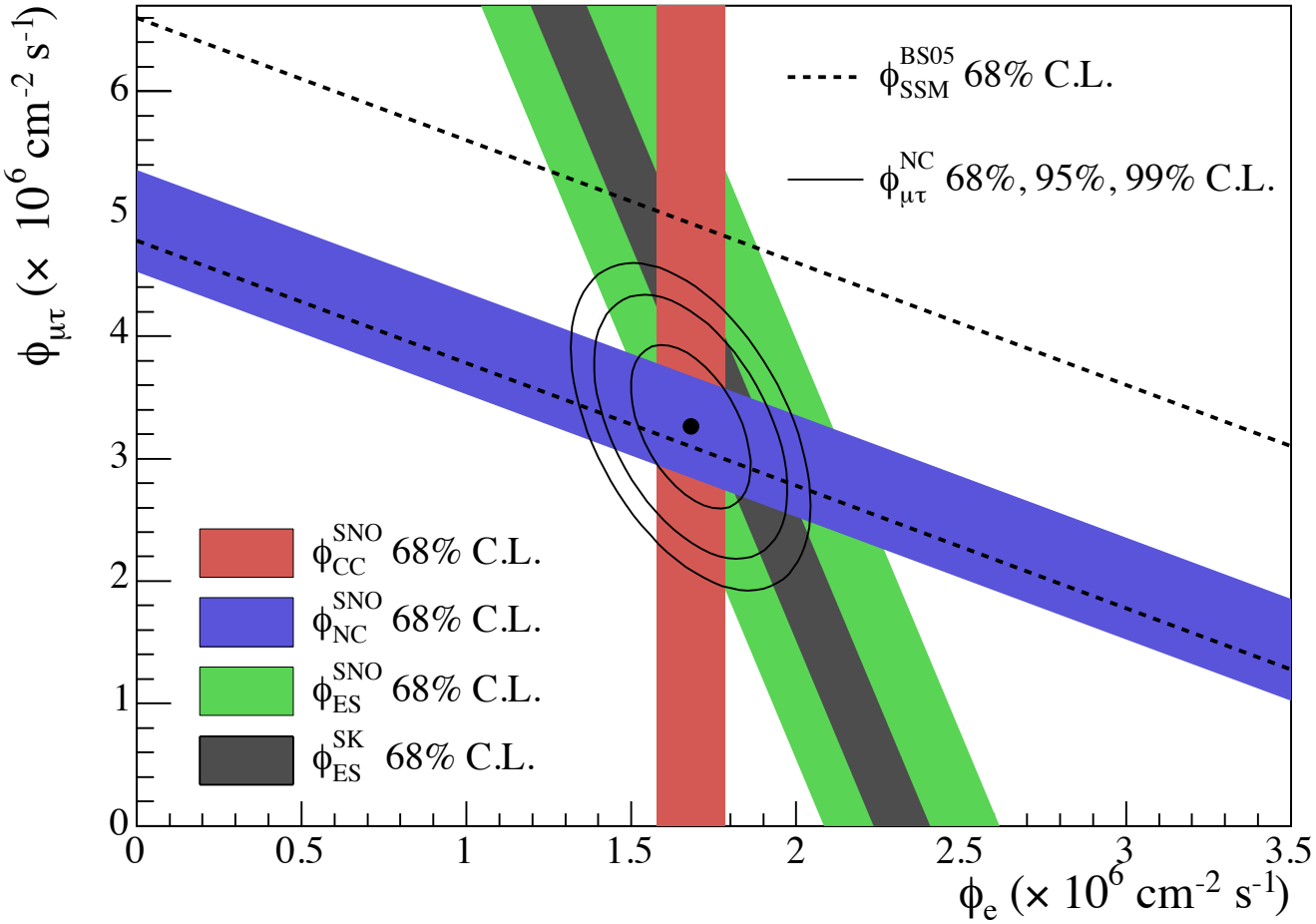

Figure 14.2: Fluxes of ^{8}B solar neutrinos, $\phi(\nu_e)$, and $\phi(\nu_{\mu,\tau})$, deduced from the SNO's CC, ES, and NC results [60]. The Super-Kamiokande ES flux is from [61]. The BS05(OP) standard solar model prediction [40] is also shown. The bands represent the 1σ error. The contours show the 68%, 95%, and 99% joint probability for $\phi(\nu_e)$ and $\phi(\nu_{\mu,\tau})$. The figure is from [60].

3 flavor oscillation formula with CP phase

$$U = \textbf{V}_{\textbf{PMNS}} = \begin{pmatrix} 1 & 0 & 0 \\ 0 & c_{23} & s_{23} \\ 0 & -s_{23} & c_{23} \end{pmatrix} \begin{pmatrix} c_{13} & 0 & s_{13}e^{-i\delta_{CP}} \\ 0 & 1 & 0 \\ -s_{13}e^{i\delta_{CP}} & 0 & c_{13} \end{pmatrix} \begin{pmatrix} c_{12} & s_{12} & 0 \\ -s_{12} & c_{12} & 0 \\ 0 & 0 & 1 \end{pmatrix}$$

$$\phi_{kj} = \frac{\Delta m^2_{kj} L}{4E}.$$

$$P(\overset{(-)}{\nu}_{\mu} \to \overset{(-)}{\nu}_{\mu}) = 1 - 4\left(s^2_{12}c^2_{23} + s^2_{13}s^2_{23}c^2_{12} + 2s_{12}s_{13}s_{23}c_{12}c_{23}\cos\delta_{CP}\right)s^2_{23}c^2_{13}\sin^2\phi_{31}$$
$$- 4\left(c^2_{12}c^2_{23} + s^2_{13}s^2_{23}s^2_{12} - 2s_{12}s_{13}s_{23}c_{12}c_{23}\cos\delta_{CP}\right)s^2_{23}c^2_{13}\sin^2\phi_{32} - 4\left(s^2_{12}c^2_{23} + s^2_{13}s^2_{23}c^2_{12} + 2s_{12}s_{13}s_{23}c_{12}c_{23}\cos\delta_{CP}\right)$$
$$\times\left(c^2_{12}c^2_{23} + s^2_{13}s^2_{23}s^2_{12} - 2s_{12}s_{13}s_{23}c_{12}c_{23}\cos\delta_{CP}\right)\sin^2\phi_{21}, \qquad ($$

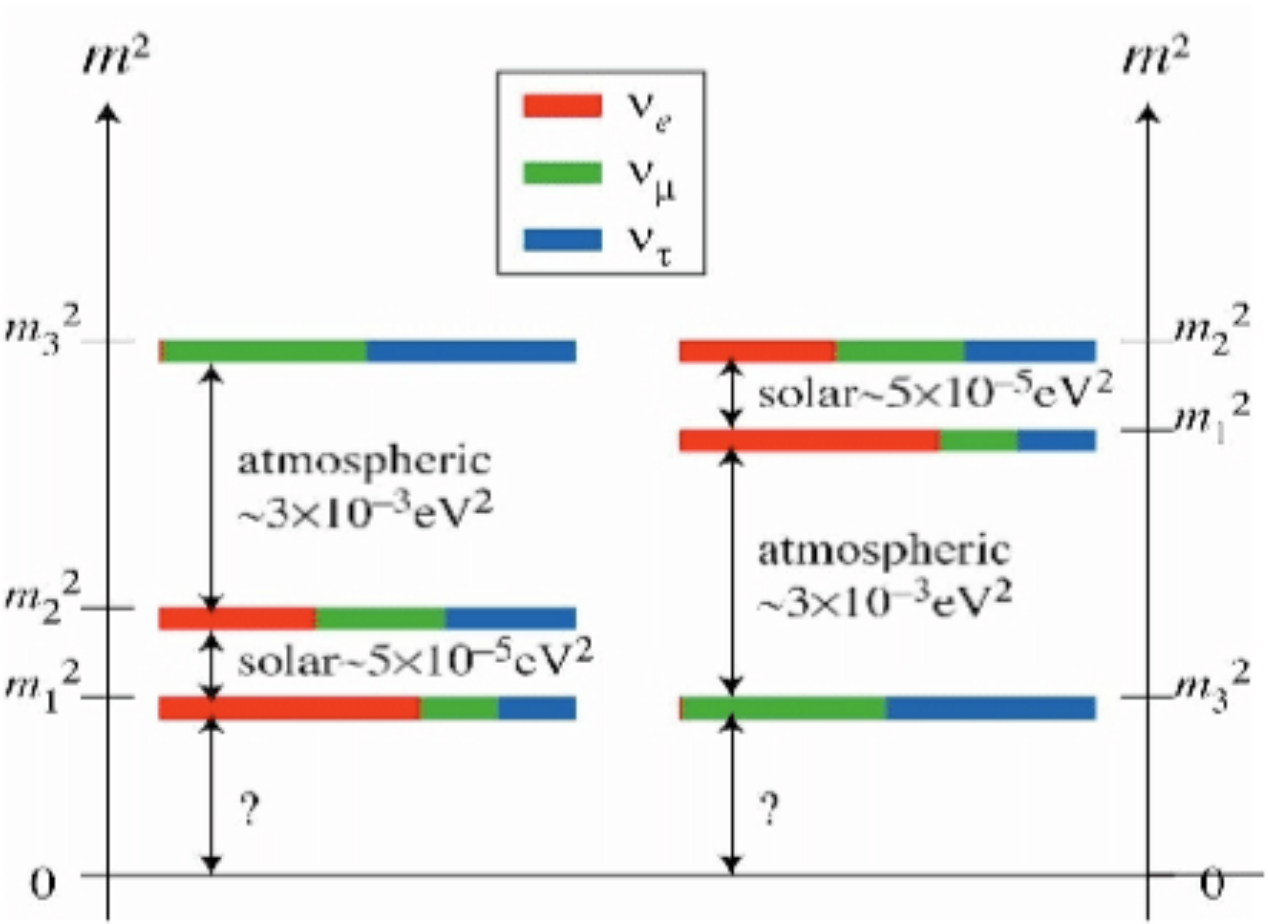

Normal hierarchy
$m_3 > m_2 \sim m_1$

Inverted hierarchy
$m_2 \sim m_1 > m_3$

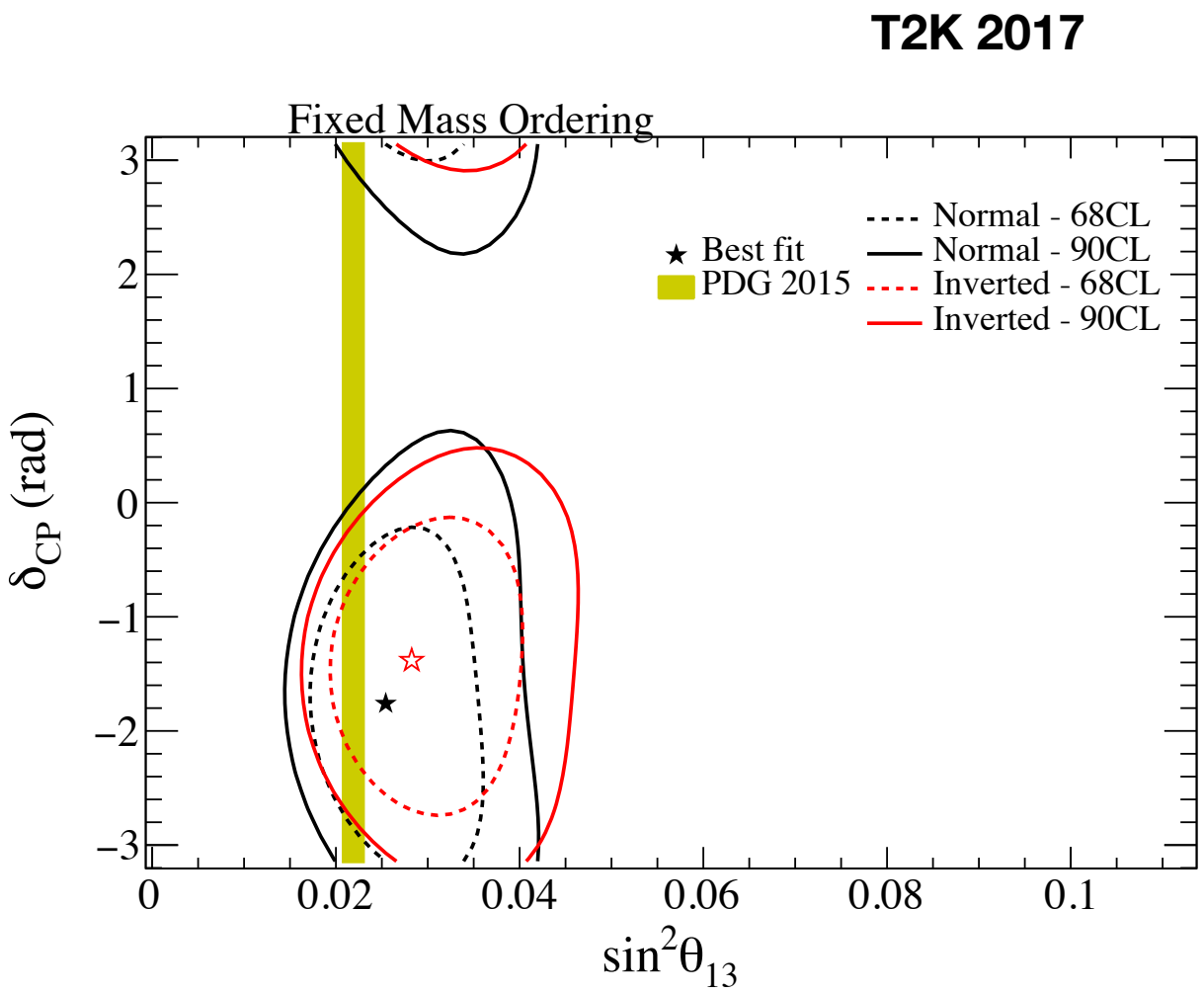

FIG. 37. Two-dimensional constant $\Delta\chi^2$ contours for oscillation parameters δ_{CP} and $\sin^2\theta_{13}$ using T2K data only. The yellow band corresponds to the reactor value on $\sin^2\theta_{13}$ from the PDG 2015 [75].

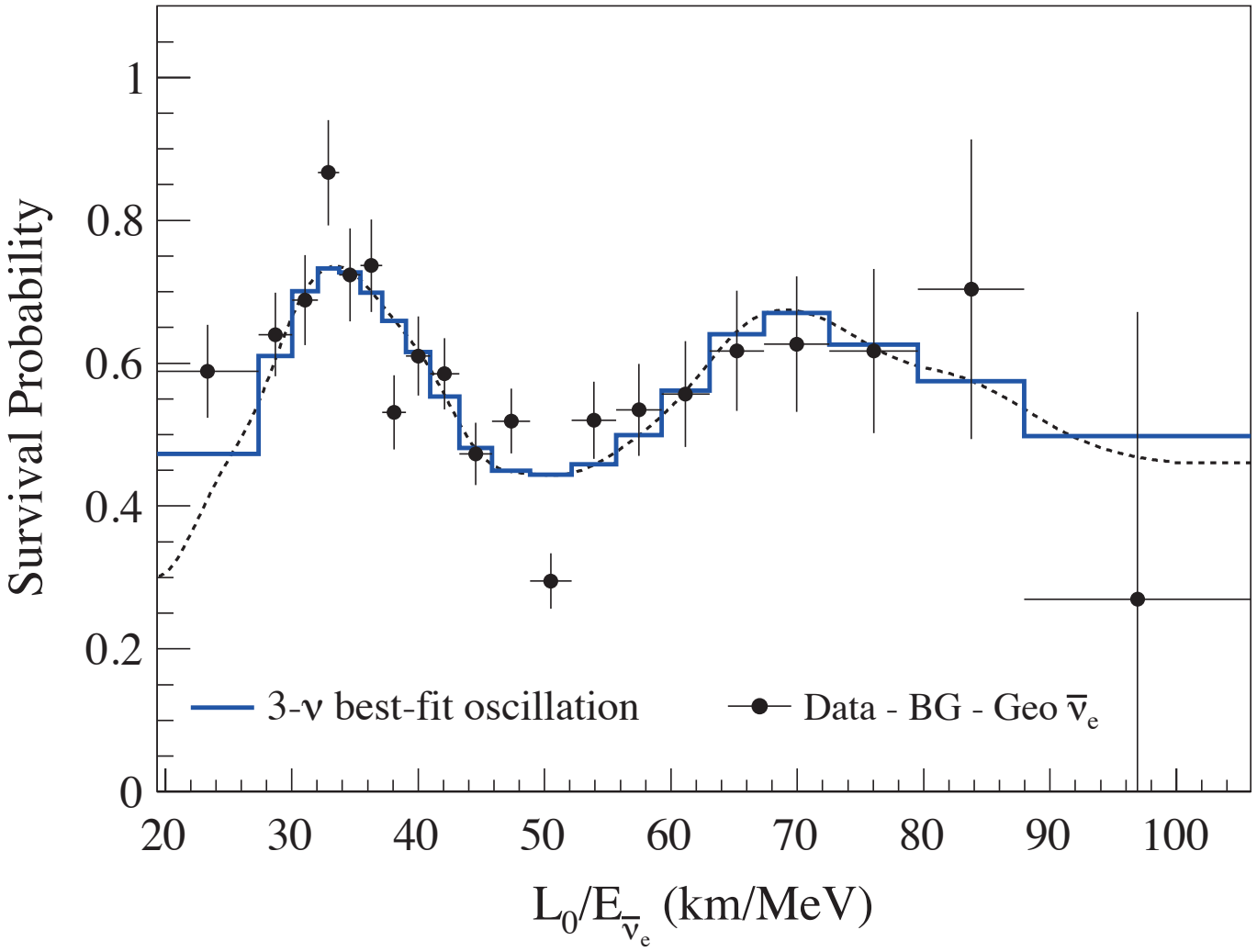

Figure 14.7: Ratio of the observed $\bar{\nu}_e$ spectrum to the expectation for no-oscillation versus L_0/E for the KamLAND data. $L_0 = 180$ km is the flux-weighted average reactor baseline. The 3-ν histogram is the best-fit survival probability curve from the three-flavour unbinned maximum-likelihood analysis using only the KamLAND data. This figure is taken from [150].

MiniBooNE 2018 requires delta m^2 > 0.25 eV^2

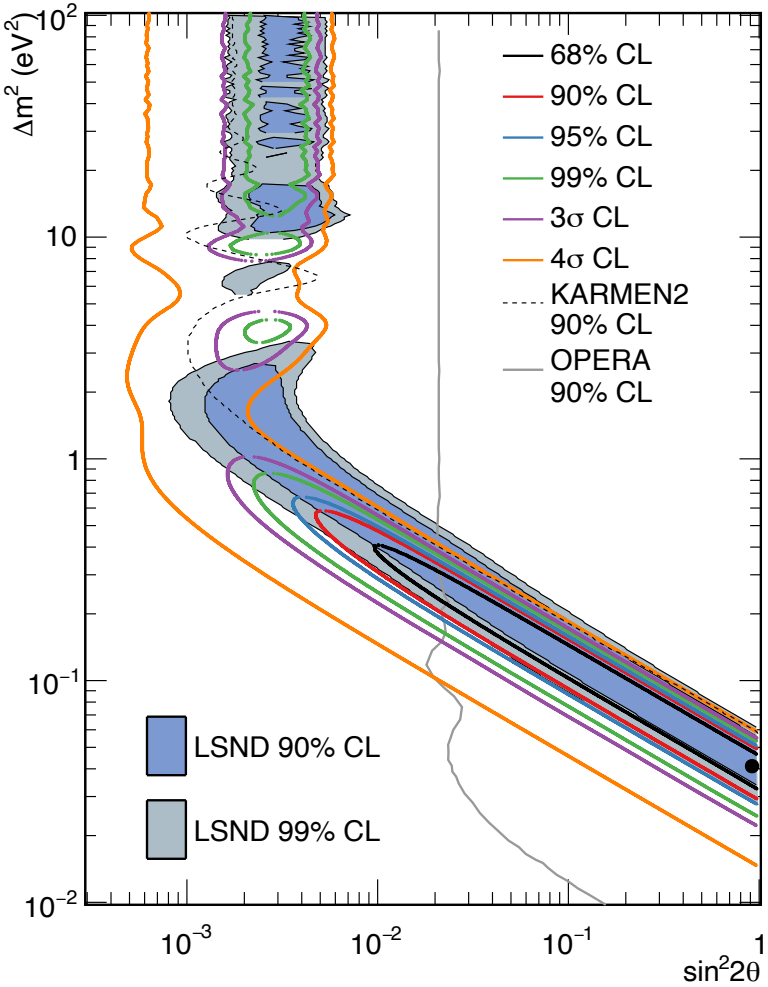

FIG. 4: MiniBooNE allowed regions for a combined neutrino mode (12.84×10^{20} POT) and antineutrino mode (11.27×10^{20} POT) data sets for events with $200 < E_\nu^{QE} < 3000$ MeV within a two-neutrino oscillation model. The shaded areas show the 90% and 99% C.L. LSND $\bar{\nu}_\mu \rightarrow \bar{\nu}_e$ allowed regions. The black point shows the MiniBooNE best fit point. Also shown are 90% C.L. limits from the KARMEN [37] and OPERA [38] experiments.

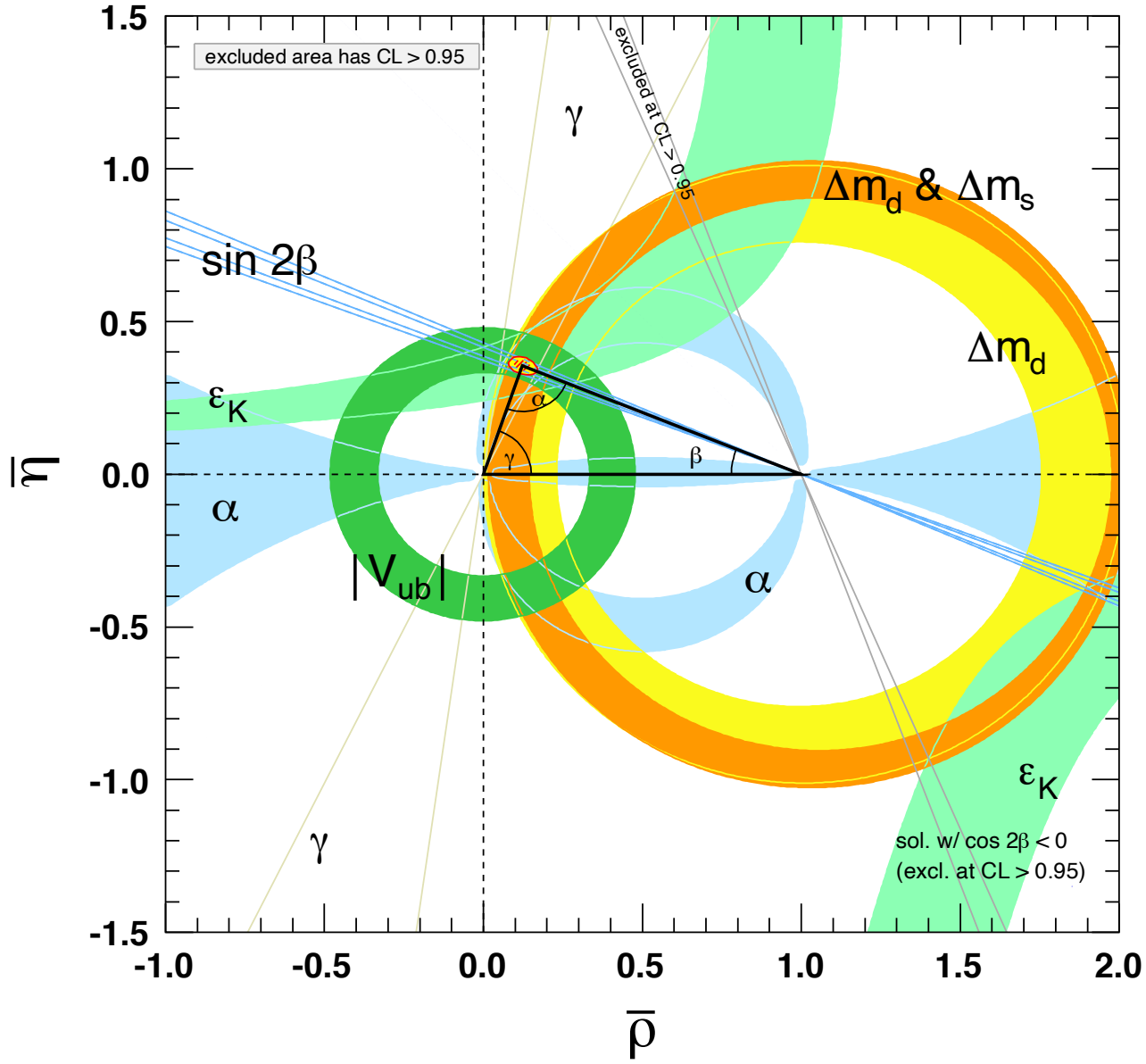

Figure 12.2: Constraints on the $\bar{\rho}, \bar{\eta}$ plane. The shaded areas have 95% CL.